Fall of ground study using seismic hazard assessment methods for an underground mine

http://dx.doi.org/10.1590/0370-44672021760061

Lucas Aguiar Vita[1,4]
https://orcid.org/0000-0002-2126-5062
Laura Frota Campos Horta[2,5]
https://orcid.org/0000-0002-2562-5686
João Pedro Alves Fraga[3,6]
https://orcid.org/0000-0002-4584-5010
Rodrigo Peluci de Figueiredo[1,7]
https://orcid.org/0000-0001-7573-7734

[1]Universidade Federal de Ouro Preto – UFOP, Escola de Minas, Departamento de Engenharia de Minas, Ouro Preto - Minas Gerais - Brasil.

[2]Universidade Federal de Ouro Preto – UFOP, Escola de Minas, Programa de Pós-graduação em Geotecnia, Núcleo de Geotecnia da Escola de Minas (NUGEO), Ouro Preto - Minas Gerais - Brasil.

[3]AngloGold Ashanti Ltd - Mina Cuiabá, Sabará - Minas Gerais - Brasil.

E-mails: [4]lucasaguiarvita@gmail.com, [5]lauralfch@gmail.com, [6]jpfraga@anglogoldashanti.com, [7]rpfigueiredo@ufop.edu.br

Abstract

This article proposes to evaluate the application of Seismic Hazard methodologies for the study of falls of ground (FOG) that occurred in the Cuiabá underground mine. Specifically, a fall of ground that occurred in 2018 in the Serrotinho mineralized body (level 18) was elected as the object of study, since it had characteristics common to other FOGs that occurred deep in the mine. Because of the close proximity and timing of the events, another three FOGs were considered in order to understand the relationship between these rock detachment events and microseismicity. Regarding seismic hazard methods, the apparent stress ratio (ASR) could provide an overview of the evolution of apparent stress in the region. The interpolation of the ASR of microseismic events to the mine levels, in 3 of the 4 cases studied, mapped the FOG region as having a high apparent stress ratio before its occurrence. A rockburst early warning methodology, in turn, proved to be helpful in the identification of precursor conditions of a microseismic event of greater local magnitude (M_L = 0.5) in the analyzed period. Although, during application of this method, some difficulties were found in identifying the right precursors patterns of the microseismic parameters.

Keywords: underground mining; microseismic monitoring; fall of ground.

1. Introduction

The Cuiabá underground mine, owned by AngloGold Ashanti, is located in the Brazilian municipality of Sabará-MG, in the northeastern part of the Quadrilátero Ferrífero mineral province (Figure 1). The mine is considered to be a world-class gold deposit and currently operates up to about 1300m below the surface, one of the deepest in Brazil (Costa *et al*., 2019). The principal mining method applied in the mine is sub-level stoping on seven mineralized bodies, standing out the orebodies with the highest oz/ton: Serrotinho (SER) and Fonte Grande Sul (FGS).

The mine's geology comprises a succession of rocks typical of the Rio das Velhas greenstone belt, more precisely the Nova Lima Group (Figure 1). A layer of banded iron formation (BIF) intercalates with mafic-ultramafic volcanic rocks and metasedimentary rocks (Ribeiro-Rodrigues *et al*., 2007). Structurally, the folding of the layers resembles the shape of a tubular cone, commonly called "Pêra".

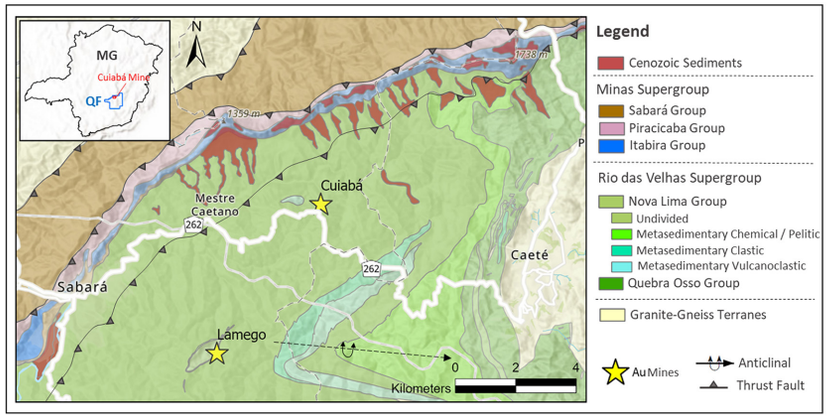

Figure 1 – Simplified geologic-structural map of the Cuiabá Mine area, at the northeastern part of the Quadrilátero Ferrífero. Modified from Endo *et al.*, (2019).

AngloGold Ashanti and the Institute of Mining Seismology (IMS) implemented the microseismic monitoring system in the Cuiabá Mine at the end of 2015 to monitor the rock mass reaction to mining in real-time. The system's configuration by 2019 included 24 geophones (16 uniaxial and 8 triaxial) ranging in depth from 600 to 1000 meters (Figure 2). Beyond the sensors, the monitoring system consists of five receiving stations, one central station, and transmission cables. All data is pre-processed in a central server before being distributed to other applications for 3D visualization and interpretation of the seismic parameters.

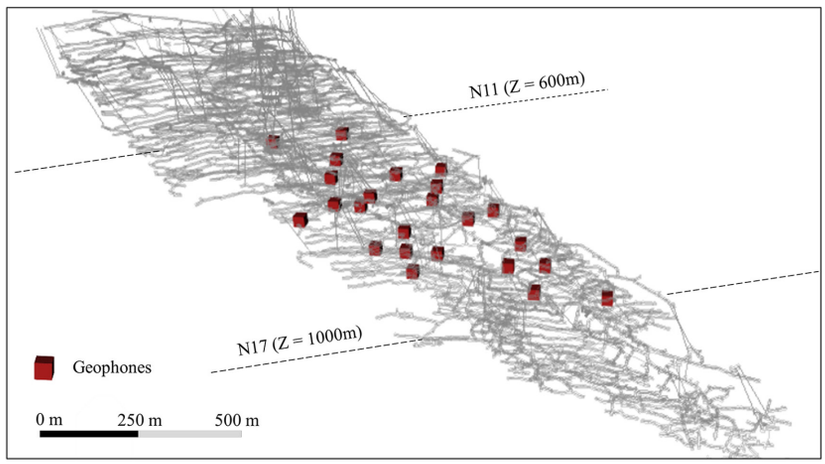

Figure 2 - Geophone's location along with Cuiabá Mine.

2. Methodology

2.1 FOG in study

Fall of ground (FOG) is a condition in which the rock detaches from the gallery's sides, pillars, or roof in an uncontrolled manner, possibly endangering people's safety or causing damage to equipment (Ma *et al.*, 2020). According to Ma *et al.* (2020), the formation process of a FOG may be the expansion and penetration of micro-cracks in the rock, resulting in fracturing and detachment. It is also worth noting the role of seismicity in amplifying these fractures and ejecting fragments (Diederichs, 2014).

In an internal report, Cuiaba's technical team conducted a statistical analysis of all FOGs in the Cuiabá Mine between 2018 and 2019. This report established the most frequent characteristic of a FOG in Cuiaba, which is: SER orebody location, below level 17, oredrive excavation type, and in the contact between BIF and Schist lithologies.

One FOG that occurred on July 19, 2018, gathered all these characteristics and was well documented by the mine crew (Table 1). Therefore, it was elected with a more straightforward analysis and great representativeness for rock detachment events deep in the mine. Based on that, the present study seeks, at first, to characterize this FOG microseismicity and seismic hazard. To accomplish that, the first step is to filter the microseismic events related to FOG.

Table 1 - Summary of the characteristics of the FOG in study.

Date	Orebody	Level	Elevation (m)	Excavation type	Lithology
July 19, 2018	SER	18	-153	Oredrive	Schist/BIF

2.2 Space-time filtering of microseismic events

Brown *et al.* (2015) mention that the choice of the time period for assessing a given area's seismic hazard depends on its rate of seismic activity and the objective of the study. Accordingly, for medium to short-term mine planning, the authors advise that a period of a few months may be used. Adopting this advice given by Brown *et al.* (2015), the microseismic data was filtered to three months before and a few days after the FOG selected happened. In this way, the objective was to identify the rock mass's dynamic and stress behavior temporally, based on the microseismic parameters. Besides this, there was also a spatial filter on the recorded microseismic events. This spatial filter aimed to restrict the analysis only to events close to the mine levels (Table 2).

Table 2 - Parameters of the filter applied to the microseismic data to restrict distant events in space and time to the FOG in study.

Date		Elevation (m)		Northing (m)		Easting (m)	
Start	End	Max	Min	Max	Min	Max	Min
April 1, 2018	August 3, 2018	-100	-250	-2050	-2240	-750	-1015

Figure 3 shows that when delimiting the data in time and space, three other FOGs were identified before the FOG selected in the present study. Each of these FOGs received an identification number according to its dates, such as FOG1(May 11, 2018), FOG2 (May 17, 2018), FOG3 (June 17, 2018), and FOG4 (July 19, 2018). Moreover, the same image highlights the region's seismic activity (109 events of local magnitude greater than -1.6 in 124 days). Therefore, the seismic hazard methodologies applied in this study attempt to understand the microseismicity and FOG correlation for all these four FOGs, since they are centered in the same cluster of microseismic events and may be correlated.

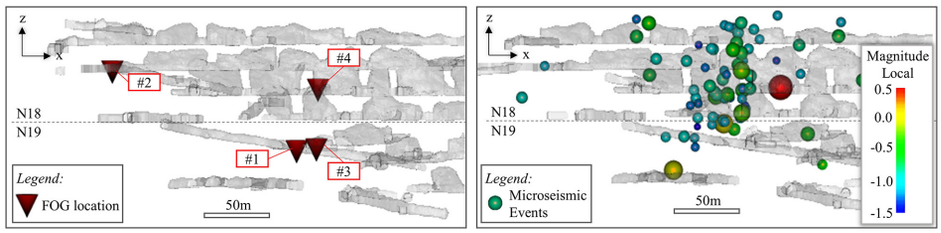

Figure 3 – The image at the left shows locations of the four FOG that took place in the level 18/19 SER orebody in the period studied: FOG#1(May 11, 2018), FOG#2 (May 17, 2018), FOG#3 (June 17, 2018), and FOG#4 (July 19, 2018). The image at the right shows seismic events in the same area colored and sized based on their Local Magnitude.

Once all the seismic data has been filtered, this work could use it for seismic hazard retro analysis of the FOG events. The methodologies chosen were the apparent stress ratio and the rockburst early warning.

2.3 Apparent stress ratio (ASR)

The use of the apparent stress ratio (ASR) in seismological risk mapping in a mine is described by Brown *et al.* (2015). The principal objective in calculating this ratio is to identify areas of increasing apparent stress as a guide to identifying rock mass in more stressed regions. It can be calculated by Equation (1):

$$ASR = \frac{\sigma_{a80}}{\sigma_{a20}} \quad (1)$$

Where: σ_{a80} = 80° percentile of apparent stress; σ_{a20} = 20° percentile of apparent stress.

The apparent stress used in the previous equation is obtained by the relationship between energy and moment of microseismic events, parameters automatically obtained by the IMS system. Its formula is defined by Wyss & Brune (1968) in Equation (2):

$$\sigma_a = \mu\,(E/M) \quad (2)$$

Where: σ_a = apparent stress (Pa = N/m^2); μ = shear modulus of the medium stiffness (N/m^2); E = seismic energy (Joules = N.m); M = seismic moment (N.m).

Brown *et al.* (2015) proposes that the ASR should be calculated over a growing event population (cumulative distribution). Thus, the ASR tells how apparent stress behaves over time, based on the distribution of past events. Therefore, it is a relative parameter rather than an absolute parameter.

2.4 Rockburst early warning

Mendecky (1997) says that the relationship between some mine seismology parameters over time may inform conditions preceding a significant dynamic event, such as a rockburst or a seismic event of greater magnitude.

The relationship between some of these parameters is best seen graphically (Figure 4). Between the parameters presented, the energy index (EI) and the cumulative apparent volume (VAC) will be used herein.

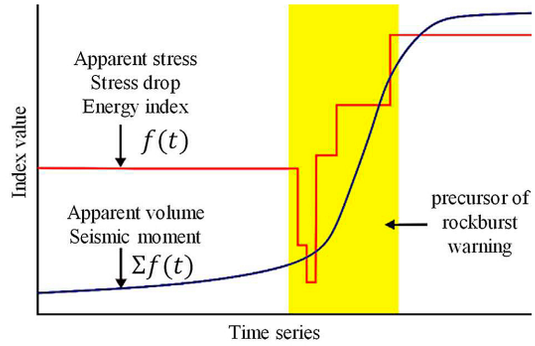

Figure 4 - Evolution of microseismic parameters that may inform a precursor condition of a rockburst or a major seismic event (Ma *et al.*, 2020).

2.4.1 Cumulative apparent volume (VAC)

The cumulative apparent volume (VAC) consists of the sequential sum of each microseismic event's apparent volume (VA) over time. The apparent volume, in turn, is related to the inelastic deformation of the rock mass, at the moment of the seismic event, concerning the apparent stress and rigidity of the rock (Dunn, 2005). Simplifying, the apparent volume quantifies the inelastic deformation in the rock by the seismic event. According to Mendecky (1997), this parameter can be given by Equation (3):

$$V_A = \frac{M}{2\sigma_a} = \frac{M^2}{2\mu E} \quad (3)$$

Where: V_A = apparent volume (m^3); M = seismic moment (N.m); σ_a = apparent stress (N/m^2); E = seismic energy (J); μ = stiffness modulus (N/m^2).

In this context, a high rate of increase in the apparent volume has been used to indicate the rise in the rock's inelastic deformation and the possibility of a significant seismic event.

2.4.2 Energy Index (EI)

Van Aswegen & Butler (1993) defined the energy index (EI) as the rate of seismic energy irradiated by an event (E) divided by the average of energy irradiated by events of the same seismic moment ($\bar{E}$ [M]), in Equation (4) and (5):

$$EI = \frac{E}{\bar{E}\,(M)} \quad (4)$$

$$\log \bar{E}\,(M) = c + d \log M \quad (5)$$

Where: E = seismic energy (Joules = N.m); M = seismic moment (N.m); c, d = coeficients obtained in energy-moment relationship.

The energy index is also an indicator of changes in the state of stress of the rock, specifically the driving stress from the seismic source during the event (Ma *et al.*, 2018). The necessary constants for its calculation are obtained by the E-M relationship and its trend line, presented in Equation (6) and Figure 5 for events in the SER orebody.

$$\log \bar{E}\,(M) = -6.0759 + 0.8504 \log M \quad (6)$$

Where: c = -6.0579; d = 0.8504.

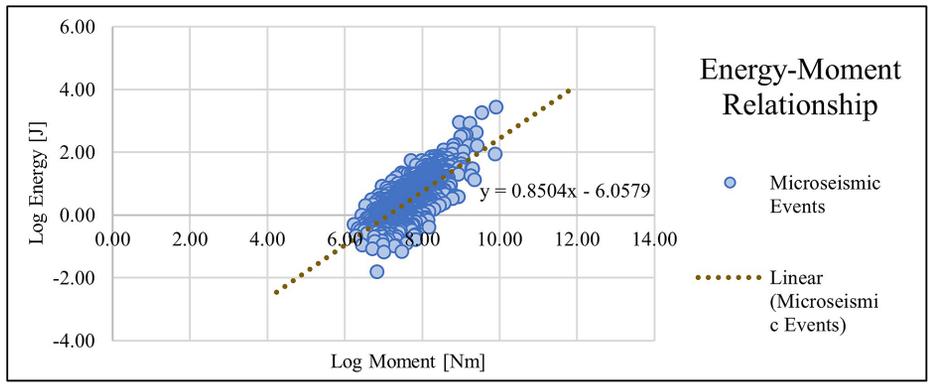

Figure 5 - Relationship between the energy values and the moment of the micro-seismic events near the FOG region under study. The linear trend line gives the constants needed to calculate the energy index (EI).

3. Results and discussion

3.1 Aparent stress ratio (ASR)

The first methodology applied to the microseismic data delimited to the FOG area was calculating the ASR. Figure 6 shows the value distribution of the ASR parameter for the filtered events.

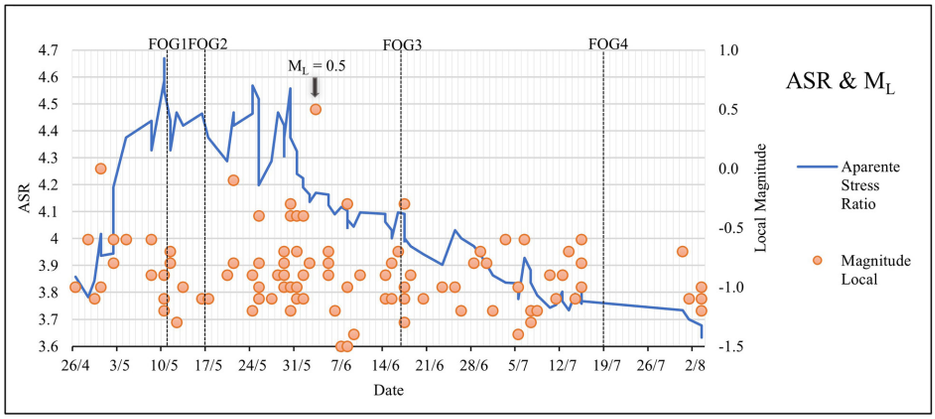

Figure 6 - Value distribution of apparent stress ratio and local magnitude for the 109 microseismic events used in seismic hazard study, between levels 18 and 19 in the SER orebody. The dotted lines show dates on which occurred a FOG in the area.

The ASR graph (Figure 6) shows that the rock mass apparent stress is constantly changing, represented by the line's tortuous path. Such behavior is expected for mining areas prone to constant changes in the stress field due to blasting and excavation, condition of the 18/19 SER at the time. Between May 10 and the beginning of June, ASR shows its maximum values, with two FOGs identified in this period. Also, at the end of May, the seismic activity rate is high, with a maximum of 5 events/day in May 30. The end of this period is marked by the biggest event of the time series, M_L=0.5 on June 3. After that, ASR show a general downtrend. This observation becomes meaningful when considering that seismic events can relieve part of the rock's existing stress.

To better understand these four FOG, each one was treated separately, observing the apparent stress ratio specific to its close area. For this, Brown *et al.* (2015) propose the interpolation of each event's ASR within a predetermined radius to assign this parameter's value to the mine's excavation boundaries, producing a map. Following the same author, the nearest neighborhood was the interpolation method used in this study, with a 30 meters search radius, since spatial adjacent microseismic events should estimate ASR values assigned to the excavation.

FOG1, FOG2 & FOG3 study

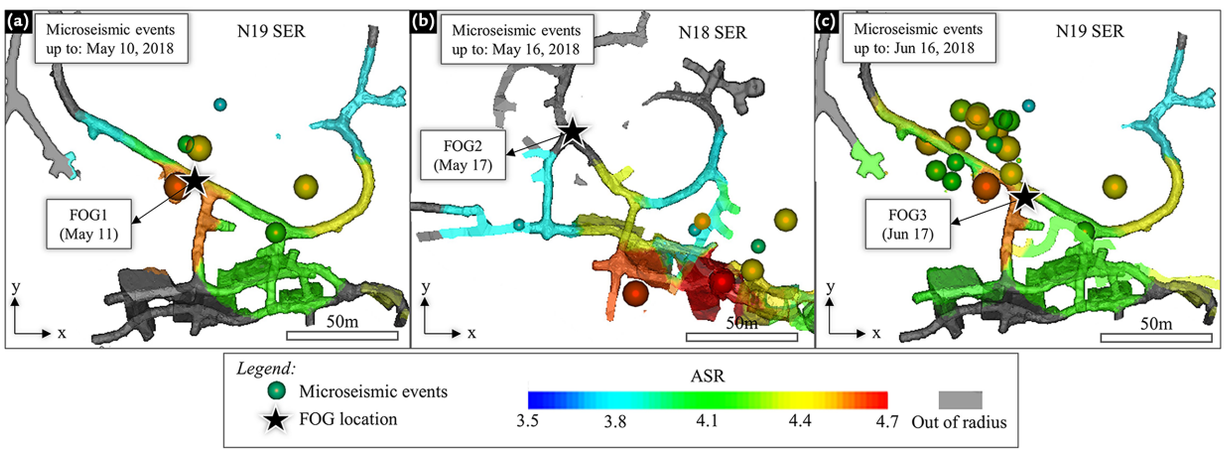

Figure 7 - Mapping of seismic hazard by the ASR parameter at levels 18 and 19 of the SER orebody, considering seismic events for the period from April 1, 2018 to 1 day before the FOG in study (located by the star): a) FOG1; b) FOG2; c) FOG3. Underground excavations were colored based on the ASR of nearby seismic events, using a search radius of 30m.

Figure 7 (a) shows the map of level 19 at Cuiaba Mine in the region where FOG1 has taken place (May 11, 2018). The map was colored according to the interpolation of the apparent stress ratio for microseismic events up to one day before FOG1. Hence, it is possible to identify that the seismic hazard map had already indicated high apparent stress in the region.

The mapping of seismic hazard to level 18, Figure 7 (b), was insufficient to determine the apparent stress condition in the FOG2 region. This occurred due to the lack of microseismic events

close to the area in the analyzed period. An alternative to estimate the region's apparent stress would be to use the nearest neighborhood interpolation with a larger sample search radius. However, this type of approach is not ideal for underground excavations, since its influence on the rock in-situ stress reaches up to 5 times the excavation radius when circular (Brady & Brown, 2006). Therefore, the apparent stress of very distant microseismic events can present values very different from those expected close to the excavation's surface and mined area. Lastly, it is worth mentioning that the FOG2 is located on an access ramp and the technical crew describes it with a relatively small concrete detachment. Thus, factors other than the microseismicity may have conditioned it.

Finally, in Figure 7 (c), can be seen that the location of FOG3 is very close to FOG1, both with a relative high ASR of approximately 4.5. Figure 6 points out that in the 38 days between these two falls of ground the ASR for the whole cluster of seismic events decreased from 4.5 to 4.1. Although, locally, the map doesn't point significant changes on the ASR. Hence, representing the ASR in 3D space led to a more correct understanding of this limited area of high apparent stress. Moreover, stands out between Figure 7 (a) and Figure 7 (c) the increase of seismicity, represented by the concentration of spheres on the map close to the FOG3.

FOG4 study

As this work initially aimed to characterize the FOG4, it will be treated in more detail. Before, it is necessary to understand how the apparent stress changes during time occurred in the region close to this FOG (Figure 8). To do that, 3 time frames were selected: the first (May 1), one month after April 1, 2018 (initial time filter); The second (June 3), 33 days after the first time frame, at the time which the M_L=0.5 took place; The third time frame (July 15), 42 days after the second time frame, 4 days before the FOG4 and also the last day which the microseismic monitoring was up for the area.

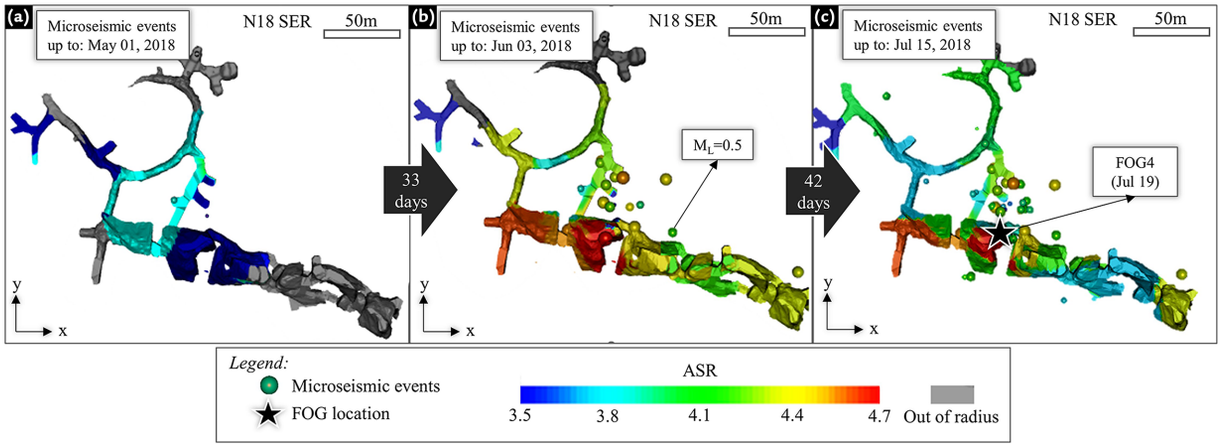

Figure 8 - Time evolution of the seismic hazard mapping by ASR to level 18, SER orebody, considering seismic events for the period from April 1, 2018, to: a) May 1; b) June 3; c) July 15. Underground excavations were colored based on the ASR of nearby seismic events, using a search radius of 30m.

Figure 8 (a) shows that, in the first month of analysis, few microseismic events in the region were detected, making it impossible to map the apparent stress condition widely. However, despite the limited data in this period, there is a low ASR identified. This situation changes considerably after one month, Figure 8 (b), when there is an increase in the rate of seismic activity and events of high apparent stress are concentrated next to 18 SER oredrive area. At June 3 follows a microseismic event of local magnitude equal to 0.5 (greatest of the period analyzed) in the same place at the mine. It is important to mention that this unique microseismic event did not increase the ASR (Figure 6), even though having a large magnitude. In the last time frame considered, Figure 8 (c), 4 days before the FOG4, is identified that most areas shows a decrease in the ratio, altough in a small area of the 18 SER oredrive the ASR stood high. This small area was also the location of FOG4.

As mentioned before, this analyses could not include microseismic events up to 3 days before FOG4. However it does exclude that the FOG4 area represented a point of attention since June 3.

The mine's technical staff descriptive report of FOG4 presents essential considerations. As a first point to be considered, the area has been excavated as an open stope, generating a large void in the rockmass. Besides, several other mine stopes were allocated and blasted in nearby regions. All of these factors may have contributed to the region remaining under high stress during this period and, consequently, the microseismicity was sensitive to this situation.

3.2 Rockburst early warning

Mendecky (1997) proposes that the relationship between some mine seismology parameters during a time, such as apparent volume and energy index, may indicate precursor conditions to rock dynamic events. To verify its effectiveness in the Cuiabá mine context, Figure 9 graphically reproduces the VAC and EI parameters' behavior throughout the occurrence of the four FOGs identified between levels 18 and 19 of the SER body.

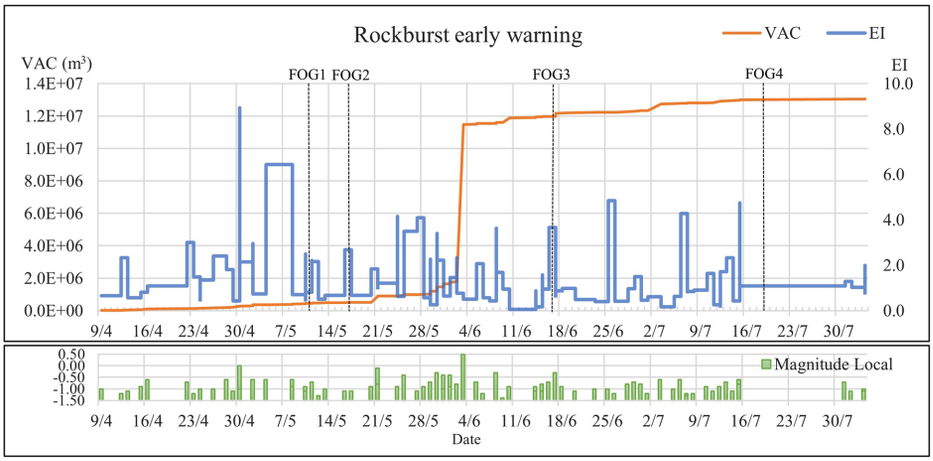

Figure 9 – Rockburst early warning chart for microseismic events at levels 18 and 19 of the SER body.

The graph in Figure 9 shows that there is a wide variation in the energy index (EI). On the other hand, the cumulative apparent volume (VAC) parameter shows small changes over time, except for an abrupt increase between June 3 and 4, 2018.

In general, the application of the short-term seismic hazard methodology proved to be incapable of explaining trends between VAC and EI that were related to FOG. In this case, the non-compatibility of the short-term seismic hazard method with the FOG analysis does not entirely exclude its potential. It is possible to identify that the abrupt increase in VAC occurs with the microseismic event of highest local magnitude recorded ($M_L = 0.5$). The graph in Figure 10 better restricts this finding in time.

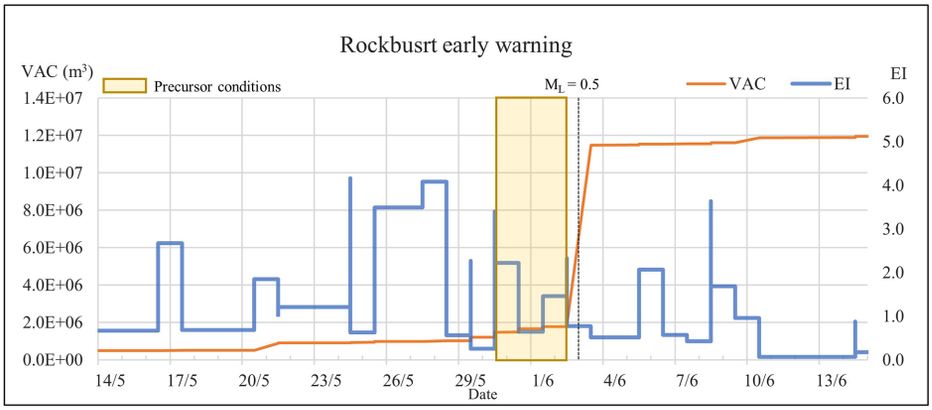

Figure 10 - Short-term Seismic hazard for the period close to the event of greatest local magnitude recorded in the study area.

Figure 10 shows that during the four days before the microseismic event of $M_L = 0.5$, the cumulative apparent volume (VAC) showed an increase in its rate. Between the 3rd and second day before the event, the energy index (EI) has a downward trend. However, this parameter starts to grow again soon after. Such EI and VAC conditions are similar to what is proposed by Mendecky (1997) to indicate that a large dynamic event may occur shortly. This forecast, in this case, was verified, when there occurred a seismic event one day later $M_L = 0.5$.

Despite the success of the methodology in retro analysis, some observations must be made. The first point is the great difficulty in identifying trends, either negative or positive, for the EI parameter (due to its significant variability). The same is true for VAC, but for the opposite reason, in which the changes are not very significant before the great seismic event. Another fact is the short period of time, about 1 to 2 days, for the precursor conditions to be identified and security actions to be taken. Finally, it must be considered that the rockburst early warning method has been used in regions prone to larger seismic events, much higher than 0.5 M_L. Therefore, stronger precursor events are captured, resulting in better consistency of microsystemic data and making it easier to identify patterns.

4. Conclusions

The microseismic monitoring system installed at the Cuiabá Mine allowed the relationship between microseismicity and FOG occurrence to be investigated. In this study, a target fall of ground and three others were studied due to the space-time proximity between them. The apparent stress ratio (ASR) proved to be an excellent tool in showing the temporal evolution of rock mass apparent stress linked to changes in the rate of seismic activity. In this sense, the interpolation of ASR value for the mine levels enabled the mapping of regions susceptible to instabilities, with an excellent correlation between FOG locations and areas of high ASR in 3 of the 4 FOGs studied. However, having said all of that, one must consider the low impact of high magnitude events on the ASR method. These events of greater magnitude, in turn, were better understood in the rockburst early warning method, capable of informing precursor conditions for significant microseismic events. Although, this methodology proved to be difficult to apply to the dataset from this article, due to the difficult to identify patterns in energy index (EI) and apparent volume (VAC) values.

References

BRADY, B. H. G.; BROWN, E. T. ***Rock mechanics for underground mining.*** 3. ed. Heidelberg: Springer Netherlands, 2006. 628 p.

BROWN, L. G.; HUDYMA, M. R.; TURCOTTE, P. Seismic hazard assessment using apparent stress ratio. *In*: INTERNATIONAL SEMINAR ON DESIGN METHODS IN UNDERGROUND MINING, 2015, Perth. ***Proceedings*** [...]. Perth: Australian Centre for Geomechanics, 2015. p. 123-134.

COSTA, L. C. B. *et al*. Support and reinforcement damage initiation and design adjustments in a deep mine environment case study: Cuiabá Mine, Minas Gerais, Brazil. *In*: INTERNATIONAL CONFERENCE ON DEEP AND HIGH STRESS MINING, 9., 2019, Johannesburg. ***Proceedings*** [...]. Johannesburg: The Southern African Institute of Mining and Metallurgy, 2019. p. 97-108.

DIEDERICHS, M. S. When does brittle failure become violent? Spalling and rockburst characterization for deep tunneling projects. In: WORLD TUNNELING CONFERENCE, 40., 2014, Foz do Iguaçu. ***Proceedings*** [...]. São Paulo: CBT/ABMS, 2014.

DUNN, M. J. Seismicity in a scattered mining environment–a rock engineering interpretation. *In*: INTERNATIONAL SYMPOSIUM ON ROCKBURSTS AND SEISMICITY IN MINES, 6., 2005, Perth. ***Proceedings*** [...]. Perth: Australian Centre for Geomechanics, 2005. p. 337-346.

ENDO, I. *et al*. ***Mapa geológico do Quadrilátero Ferrífero, Minas Gerais, Brasil.*** Escala 1:150.000. 2019. 1f. Centro de Estudos Avançados do Quadrilátero Ferrífero - Escola de Minas - UFOP, Ouro Preto, 2019. Disponível em: https://www.qfe2050.ufop.br. Accesso em: 1 jun. 2021.

MA, C.; LI, T.; ZHANG, H. Microseismic and precursor analysis of high-stress hazards in tunnels: a case comparison of rockburst and fall of ground. Engineering Geology, v. 265, p. 105435, 2020.

MA, T. *et al*. Rockburst mechanism and prediction based on microseismic monitoring. ***International Journal of Rock Mechanics and Mining Sciences,*** v. 110, p. 177-188, 2018.

MENDECKI, A. J. ***Seismic monitoring in mines.*** Heidelberg: Springer Netherlands, 1997. 262 p.

REBULI, D. B.; VAN ASWEGEN, G. Short term Seismic hazard assessment in SA Gold Mines. *In*: INTERNATIONAL SYMPOSIUM ON ROCKBURSTS AND SEISMICITY IN MINES, 8., 2013, Saint-Petersburg. ***Proceedings*** [...]. Obinisk: GS RAS & MI UB RAS, 2013. p. 323-331.

RIBEIRO-RODRIGUES, L. C.; DE OLIVEIRA, C. G.; FRIEDRICH, G. The Archean BIF-hosted Cuiabá Gold deposit, Quadrilátero Ferrífero, Minas Gerais, Brazil. ***Ore Geology Reviews***, v. 32, n. 3-4, p. 543-570, 2007.

VAN ASWEGEN, G.; BUTLER, A. G. Applications of quantitative seismology in South African gold mines. ***Rockbursts and Seismicity in Mines,*** v. 93, p. 261-266, 1993.

WYSS, M.; BRUNE, J. N. Seismic moment, stress, and source dimensions for earthquakes in the California Nevada region. ***Journal of Geophysical Research,*** v. 73, n. 14, p. 4681-4694, 1968.

Received: 15 August 2021 - Accepted: 2 March 2023.